Annals of Clinical and Medical Case Reports

DOI: http://dx.doi.org/10.47829/ACMCR.2020.5601

Research Article

ISSN 2639-8109 | Volume 5

Molecular Signature and Anatomical Features of a Hypertrophic Scar From Abdominal Skin of a 36-Year-Old Female

Hameed S and Zare RN*

Department of Chemistry, Fudan University, Shanghai, 200438, China

***Corresponding author:**

Richard N. Zare,
Department of Chemistry,
Fudan University, Shanghai, 200438,
China, E-mail: rnz@stanford.edu

Received: 17 Dec 2020
Accepted: 01 Jan 2021
Published: 07 Jan 2021

Citation:

Zare RN. Molecular Signature and Anatomical Features of a Hypertrophic Scar From Abdominal Skin of a 36-Year-Old Female. Annals of Clinical and Medical Case Reports. 2021; V5(6): 1-8.

Keywords:

Human skin; Hypertrophic scar; Phospholipids; Metabolites; DESI-MSI

1. Abstract

Hypertrophic scarring is formed as a result of abnormal wound healing. Efforts have been made to understand the mechanism of hypertrophic scarring for prevention and treatment, mainly by using several model systems. However, animal models do not form effectively hypertrophic scars. Desorption electrospray ionization mass spectrometry imaging enabled label-free elucidation of the spatial distribution of metabolites and lipids in skin tissue samples under ambient conditions of a 36-year-old female. It revealed up-regulation of phospholipid sphingomyelin SM(18:0/16:1), *m/z* 235.18, and metabolite sphingosine, *m/z* 310.24, which resulted in skin hardness and defects in the skin barrier function. The scar tissue also showed downregulation of phospholipid cardiolipin CL(62:2), *m/z* 1322.03 that indicated defects in autophagy function. These findings were supported by histopathological evaluations of scar tissue which showed enlarged, disordered keloidal collagen bundles in the deep dermis. Moreover, the scar tissue showed defects in autophagy function and inflammation. Although, limited by sample number, our results clearly revealed a molecular signature of hypertrophic scarring in this human case study.

2. Introduction

Skin tissue helps the body to maintain its dynamic constancy [1], and healing ability. Wound healing is a complicated process that involves generation of multiple cell types [2,3] that undergo inflammation, proliferation, and remodeling [4]. At the site of injury keratinocytes migrate from the edge of wound into the epidermis, the immune system becomes activated, and macrophages initiate wound healing.

Scars are the result of genetic predisposition and injuries [5], that disturb the quality of life physically and psychologically [6, 7]. The plausible links between macrophages, fibrogenic mediator transforming growth factor-beta, endothelial growth factor (VEGF-A), and hypertrophic scar formation have been reviewed recently [8,9]. During the initial phases of wound healing pro-inflammatory macrophages produce interleukin-6 (IL-6), interleukin-12 (IL-12), tumor necrosis factor-α (TNF-α), and chemokineligand2 (CCL2) that act as proinflammatory cytokines and chemokines [8]. During the remodeling process anti-inflammatory macrophages are produced that generate interleukin-10 (IL-10), transforming growth factor-β1 (TGF-β1), hemeoxygenase-1 (HO-1), and arginase. These heal the wound and regenerate tissue [10]. The purpose of anti-inflammation is to halt cell damage and promote cell repair, but prolonged inflammation results in delay of wound healing. Studies have shown that the metabolites of *omega-6* fatty acids are pro-inflammatory, whereas, *omega-3* fatty acids are anti-inflammatory in nature and are involved in wound healing [11]. Moreover, defects in the macrophage functions result in increased deposition of collagen and activation of myofibroblasts that promote fibrosis [12]. The increased deposition of collagen, invasive growth of fibroblasts, and decrease of cutaneous fat and hair follicles result in scar formation [13].

Hypertrophic scar formation is a complex process, and the underlying mechanism is not completely known; therefore, the number

of preventative and therapeutic measures are limited [14]. Hypertrophic scar is inflammatory disorder of reticular skin [15], can cause severe functional and cosmetic disabilities, and is routinely characterized by microscopic observations of thin tissue sections. However, histology alone is unable to reveal the biomolecular background of the scar [16]. Efforts have been made to understand the mechanism of hypertrophic scar formation mainly by using *in-vivo* models for phenotype, whereas *in-vitro* models for identification of pathways and drug development [17]. However, these models are not ideal for the study of hypertrophic scarring. Despite many efforts the *in-vitro* models do not form hypertrophic scars effectively [18,19]. Therefore, the origin and underlying mechanism of hypertrophic scar has not been fully established. It is important to find new therapeutic targets for treatment and remediation, but these efforts are hampered by the lack of noninvasive anti-scarring therapies.

This study demonstrates a promising potential strategy for further elucidating the molecular basis of hypertrophic scar formation. Mass spectrometry has emerged as a powerful technology for rapid and precise detection of complex molecular species [20,21]. Desorption electrospray ionization mass spectrometry imaging (DESI-MSI), enabled label-free elucidation of the spatial distribution of metabolites and lipids in tissue sections at ambient conditions without any pretreatment [22,23]. The data revealed high throughput detection of metabolites and lipids that resulted in formation of hypertrophic scars. We recognize that our study is preliminary and limited, necessitating the analysis of multiple samples and control sets. Nevertheless, these findings of lipid composition may provide insights into the treatment and prevention of hypertrophic scar formation.

3. Material and Methods

Abnormal wound healing results in the formation of hypertrophic scars [25]. A 36-year-old female had scar on abdomen that was raised within a boundary. Surgical revision of scar was performed with her consent, and the scar along with some normal skin to serve as a control were made available for study **(Figure S1)**.

3.1. Collection of Tissues Microscopic Observations

Discarded scar tissue and normal adjacent skin were obtained from a 36-year- old female patient undergoing scar revision surgery in the Department of Plastic and Reconstruction Surgery, Zhongshan Hospital of Fudan University, Shanghai, China. The procedures for tissue collection were approved by the ethical code of Fudan University Hospitals in accordance with the Declaration of Helsinki Principles. Prior to surgery the patient provided informed consent. The tissue specimens were immediately frozen, prior to cryosectioning. 10 µm thin cryo-sections were prepared using Leica CM1950 Cryostat Microtome, and were mounted on glass slides provided by Tansol, China. The mounting temperature was set at -21 °C and the chamber temperature at -22 °C.

3.2. Histological Evaluations

The human skin tissues were subjected to Hematoxylin & Eosin (H&E) staining, and Congo red staining for histological evaluation. The H&E staining kit were obtained from Solarbio Life Sciences (Cat# G1120), and Congo red dye was obtained from Ruibao and Biotech Co., Ltd (Cat# R1029). For immunohistochemical analyses the following antibodies and materials were used: Beclin-1 autophagy marker (Reego and Biology, 1:200), IBA-1 inflammation marker (Reego and Biology, 1:100). HRP-labelled Goat anti-rabbit secondary antibody (Reego and Biology, 1:200), DAB (DAKO, K5007), Normal rabbit serum (Boster, AR1010), and BSA (Solarbio, A8020). High-resolution optical images of the stained tissues were recorded by an Olympus CKX53 microscope using Olympus cellSens 2.1 [ver.2.1] imaging software (Olympus, Tokyo, Japan).

3.3. Desorption Electrospray Ionization Mass Spectrometry Imaging (DESI-MSI)

The DESI-MSI source was controlled by OmniSpray 2-D (Prosolia, Inc), and was coupled with Velos Pro Ion Trap Mass Spectrometer (Thermo Scientific, USA) for imaging of human skin tissues. The spray head was made using a precision-cleaved emitter 50 µm ID x 150 µm OD x 40 mm long. The solvent line tubing had dimensions of 75 µm ID x 150 µm OD. The spray tip-to-surface distance was ~1 mm, spray incident angle of 58°, and spray-to-inlet distance ~5 mm. MS Data acquisition was performed using XCalibur 2.2 software (Thermo Fisher Scientific Inc.). The nitrogen pressure was set at 1.02 MPa; spray voltage was 4 kV, the capillary temperature at 275°C, and -Lens RF Level at 60.6%. The human skin tissue samples were analyzed in the positive ion mode. The histology compatible solvent used for both ion modes was dimethylformamide/acetonitrile (DMF + ACN) (1:1, v/v) [23] obtained from Fisher Chemical NJ, at flow rate of 1 µL/min. The data files (.raw) were exported to FireFly 3 software (Prosolia Inc.) that extracted and built the data set into (.ibd and .imzML) formats. msIQuant software was used to convert imzML data files to msiQuant readable format to view and analyze mass spectrometry imaging data [26]. The ion images used a Synapt blue-red-yellow color map. Yellow and red show high intensity signal, whereas black represents no signal.

3.4. Extraction of Biomolecules from Skin Tissue

Fragments of tissue from normal and scar skin were taken into tubes, and 3 ml of mixture of chloroform and methanol (2:1) was added into each tube, that was followed by vortex. For the surface extraction of lipids from tissues by phase separation, water was added (5-fold) into each tube that was followed by vortex and centrifugation. The organic layer was separated; it contained lipids with hydrophobic nature. Residual lipids were extracted by the ad-

dition of chloroform, methanol, water mixture (8:4:3) by repeating the steps thrice, to obtain the total lipid extract [26]. The extraction procedure produced organic fractions from each sample that were dried in the vacuum evaporator at 25 °C for around 30 minutes. The aqueous fractions were separates, centrifuged, transferred into new tubes, and dried. The samples were then stored at -20 °C until analysis. The residues were dissolved in methanol that was followed by vortex, sonication, and centrifugation. For analysis in the positive ion mode 0.5 % formic acid was added into each sample.

3.5. Electrospray Ionization Mass Spectrometry Analysis of Tissue Extract

ESI-MS is a soft ionization technique that seldom disrupts the chemical integrity of molecules in samples during analysis. Samples were introduced through a capillary tube into the Orbitrap Elite mass spectrometer (Thermo Fisher). The instrument was operated using the Orbitrap Elite software (Tune Plus 2.7). The data acquisition and processing were performed by Thermo Xcalibur (software version 3.0).

3.6. MS Settings

The organic and aqueous fractions of the samples were analyzed at the positive and negative ion modes. The heated ESI source settings were: Heater temperature: 50 °C, Sheath gas flow rate: 16 (arb), Auxillary gas flow rate: 8 (arb), Spray voltage: 4 kV for negative ion mode and 5 kV for positive ion mode was applied to the capillary that generated an electric field gradient for the movement of charged microdroplets into the mass spectrometer for analysis. Capillary temperature was set at 275 °C, and the S-Lens RF Level at 60.6 %. The Syringe pump flow rate was set at 5 µl/min. The Define Scan window was set at, Analyzer: FTMS, Mass range: Normal. The scan range for organic fractions was set at *m/z* 50 to *m/z* 1000, while the aqueous fractions were analyzed with the maximum scan value set at *m/z* 2000. The resolution was set at 120,000, Scan type: full, Microscan: 1, and Maximum injection time at 400 ms.

3.7. Identification of Phospholipids and Metabolites

The lipids and metabolites were identified by database search including LIPID Maps structural database (LMSD) (http://lipidmaps.org/data/structure/LMSDSearch.php?Mode=SetupTextOntologySearch), and Human Metabolome Database (HMDB) search engines (http://www.hmdb.ca/spectra/ms/search).

4. Results and Discussion

4.1. Surgical Revision of Scar

A number of studies have been conducted mainly by using several *in-vivo* and *in-vitro* model systems, but these are not ideal to study hypertrophic scar [17]. What might make the present study of special interest is the study of human skin instead of a model organism for direct evaluation of scar tissue sample from abdomen of a 36-year-old female after surgical revision with her consent to use the samples for research. The physical examination of patient by the physician found that normal skin was soft **(Figure S1A)** as compared to scar that was deformed, hard and rigid (**Figure S1B**) and suggested case of hypertrophic scar. Hypertrophic scar restricts growth of tissue, and movement of appendages [27]. Previous studies have shown that prolonged wound healing may undergo oxidative stress, which leads to alterations of gene expression and damages in the cell membrane and its organelles causing hypertrophic scar formation [27]. A recent study has shown that fibroblasts derived from marginal and central areas of hypertrophic scar exhibit different properties that makes understanding of hypertrophic scar more complex and its treatment more difficult [29]. Surgical scar revision procedures are being used for improvement of hypertrophic scars. Therefore, it is essential to understand the disfiguring maladaptive process of scar formation to control and assist in treatment of the pathology.

4.2. Profiling of Lipids and Metabolites in Skin Characteristic of Hypertrophic Scar Formation

Clinically effective antiscar therapies are very limited [30]. The long-term goal of the study is to identify new therapeutic targets for reducing scarring. Fig. 1A shows microscopic optical images of the surgically removed scar skin, and Fig. 2B shows normal tissue (control) of the patient.

Molecular profiling of normal skin tissue (control) and scar sample was performed by desorption electrospray ionization mass spectrometry imaging (DESI-MSI), recorded in positive ion mode. The metabolites and lipids detected from the limited number of normal skin (control) and scar skin from one individual hindered the ability to detect statistically significant results. Nevertheless, we did find that the mass spectra from the two groups showed significant differences in the abundance of metabolites and lipids as shown in 2D chemical maps (ion images) created using msIQuant software [24]. Phospholipids are the main constituents of cell membranes and sub-cellular components [31]. They are involved in cell growth and differentiation. Alterations in composition of membrane phospholipids affects the transport of molecules between cell membrane and its organelles [32] and can result in disease states [33]. The physical examination of the scar tissue showed hardness as compared to adjacent skin that suggested involvement of sphingomyelin based on previous reports, and was thus easily selected from the list of predicted metabolites by human metablome data base search. Hypertrophic scar tissue showed upregulation of phospholipid sphingomyelin SM(18:0/16:1), *m/z* 235.18 **(Figure 2A)**, as compared to normal skin (control) **(Figure 2C)**. The structural formula has been shown in **(Figure 2E)**. Sphingomyelin transports cholesterol from cell surface into the cytoplasmic organelles [34,35]. We suggest that the upregulation of sphingomyelin SM(18:0/16:1), *m/z* 235.18 in the scar tissue might lead to hardness of the tissue that was observed during physical ex-

amination of the patient before surgery. It is supported by previous report that suggested upregulation of sphingomyelin result in skin hardness and pathology [36]. Moreover, the scar tissue showed up-regulation of sphingosine, *m/z* 310.24 **(Figure 2B)** as compared to normal (control) **(Figure 2D)**. The structural formula has been shown in **(Figure 2F)**. The details of the other molecules detected by DESI have been summarized in **(Table S1)**.

Moreover, ESI-MS analysis of the normal skin (control) detected cardiolipin CL(62:2), *m/z* 1322.03 **(Figure 3A)**, that was downregulated in the scar **(Figure 3B)**. The details of the other molecules detected by ESI-MS has been summarized in (**Table S2)**. Previous studies have shown that cardiolipin resides on mitochondrial membranes and controls targeted removal of damaged mitochondria through autophagy [37]. Autophagy is essential for removing damaged organelles and misfolded proteins that delays aging. The downregulation of CL(62:2), *m/z* 1322.03 indicated defects in the autophagy function in the scar tissue. Previous studies have shown that defects in autophagy results in ailments [37], including nerve damage [38], myopathy [39], and cancer [40].

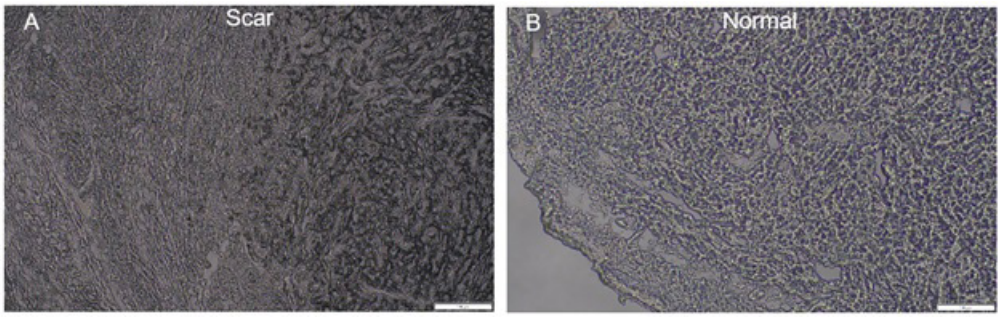

Figure 1: Microscopic optical images of the skin tissue sections. (A) Scar tissue showed abnormal texture, as compared with (B) normal skin (control) that showed no abnormality. Scale bar: 100 µm.

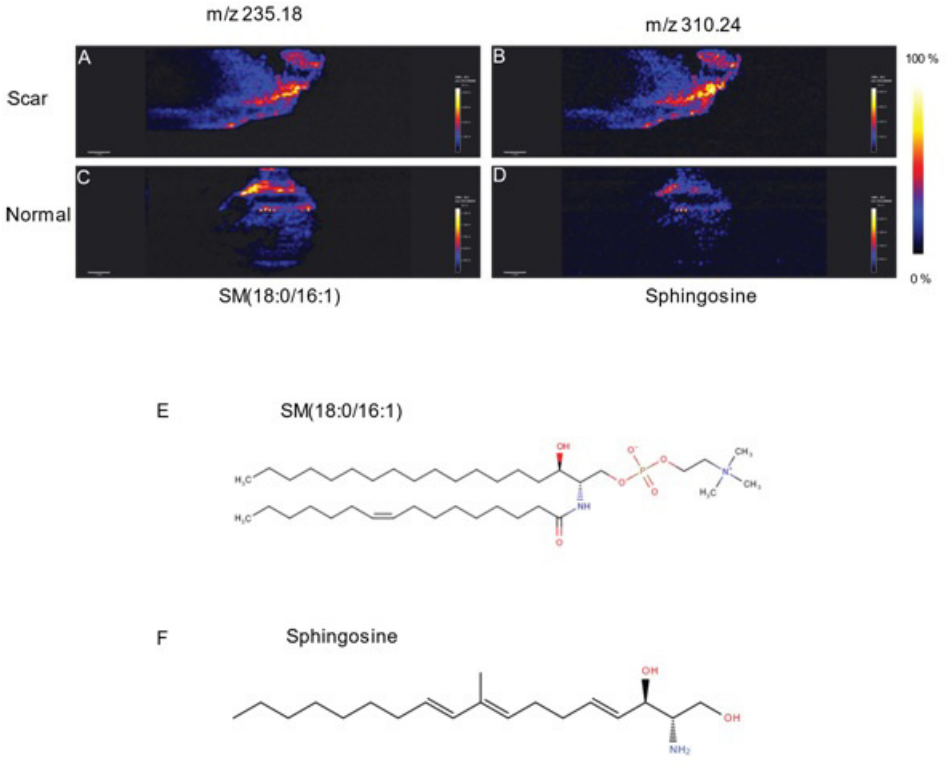

Figure 2: Profiling of lipids and metabolites in human skin scar, determined by DESI-MSI. (**A, B**) Scar tissue showing up-regulation of lipids and metabolites, as compared with (**C, D**) normal skin (control). Colour bar: Yellow and red show high intensity signal, whereas black represents no signal. Scale bar: 1 mm. Structural formula of phospholipid sphingomyelin was accessed from Human Metabolome Database (HMDB ID: HMDB0013464), and structural formula of metabolite sphingosine was accessed from Lipid Maps database (LM ID: LMSP01080014). (**E**) Sphingomyelin SM(34:1), *m/z* 235.18, and (**F**) Sphingosine, *m/z* 310.24.

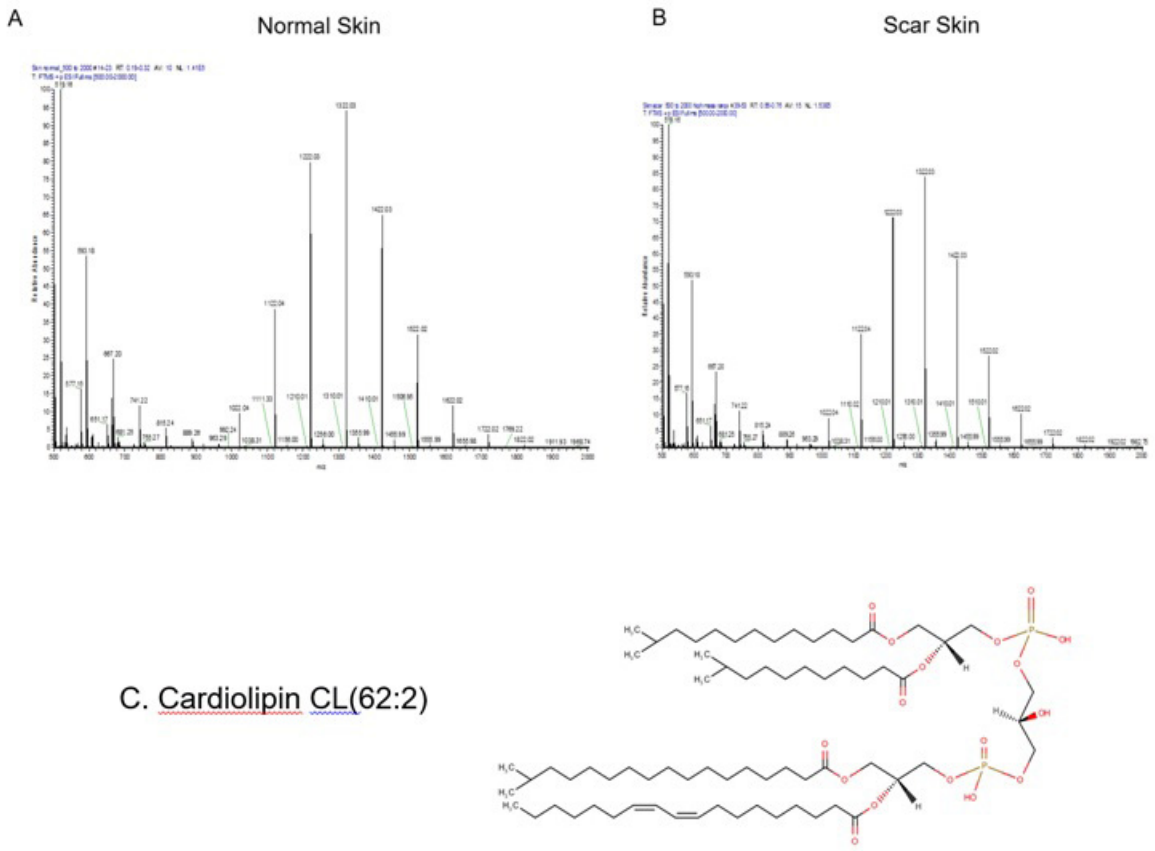

Figure 3: Scar tissue showed down-regulation of phospholipid cardiolipin. (A) Mass spectrum from normal skin tissue (control), and (B) mass spectrum from scar. (C) Structural formula of phospholipid cardiolipin CL(62:2), m/z 1322.03 accessed from Human Metabolome Database (HMDB ID: HMDB0075764).

4.3. Histological evaluation showed pathological sample was of hypertrophic scar

4.3.1. Nodule like Structures in the Deep Dermis

Haematoxylin and eosin (H&E) staining of tissues revealed the anatomy of the deep dermis. The scar tissue showed nodule-like structures **(Figure 4A-4D)**, as compared to normal skin (control) that showed no abnormality **(Figure 4E-4H)**. The histopathological evaluation of the tissue revealed that it was a hypertrophic scar. Our observation is supported by previous studies that have shown nodule-structures in the deep dermis are associated with hypertrophic scarring [41-45].

4.3.2. Disordered Arrangement of Collagen Bundles, Defects in Autophagy Function and Inflammation in Scar

Histological examination of skin tissues with Congo red staining detected no abnormality in normal skin dermis (control) **(Figure 5A)**. Whereas, the scar tissue section showed aggregates of blood vessels, as well as thick and stretched collagen bundles in abundance aligned in plane with the epidermis **(Figure 5B)**. This observation is supported by previous study that has suggested that increased deposition of collagen, and invasive growth of fibroblasts result in scar formation [13]. Immunohistochemistry of the skin tissues with the autophagy marker Beclin-1 antibody found no abnormality in the normal skin (control) **(Figure 5C)**, but detected cellular debris in scar tissue that suggested defects in the autophagy function **(Figure 5D)**, and is supported by other observation made in this study that showed downregulation of phospholipid cardiolipin CL(62:2), *m/z* 1322.03, in the tissue extracts of hypertrophic scar **(Figure 3B)** as compared to normal skin (control) **(Figure 3A)** that also suggested defects in the autophagy function. Immunohistochemistry of the skin tissues with the inflammation marker IBA-1 antibody found no abnormality in the normal skin tissue (control) **(Figure 5E)**, and detected aggregates of inflammatory cells in the scar tissue that suggested prolonged inflammation **(Figure 5F)**. It is supported by previous study that has suggested that hypertrophic scar is an inflammatory disorder of reticular skin [15].

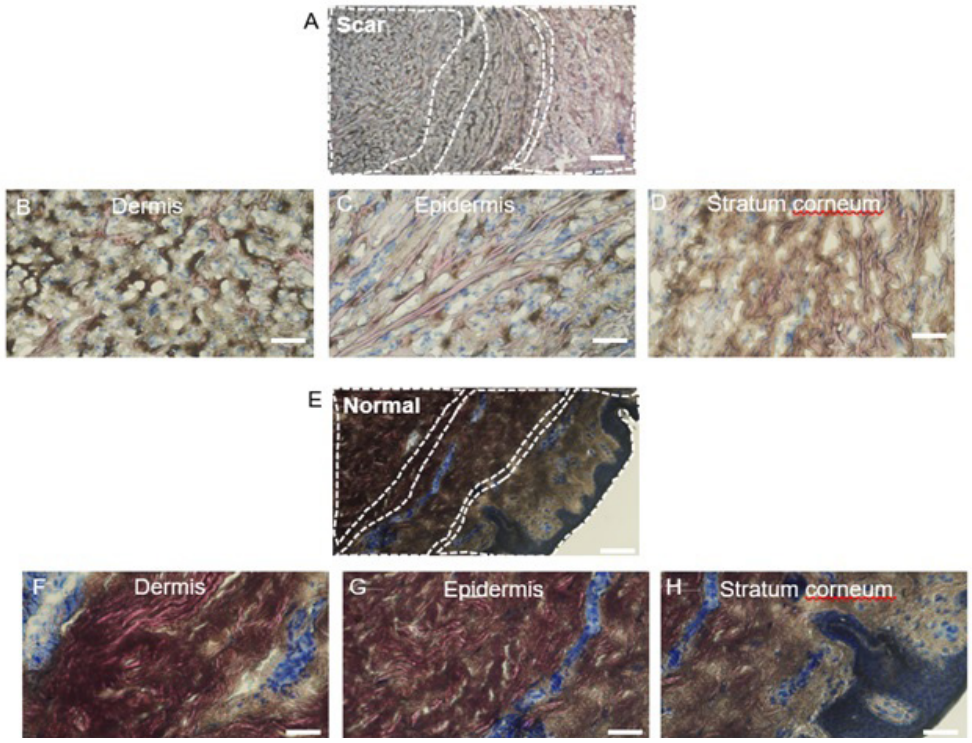

Figure 4: Histopathological evaluation of tissues with H&E staining. (**A-D**) scar tissue showed nodule-like structures in the deep dermis, as compared to (**E-H**) normal skin tissue (control) that showed no abnormalities. Magnification: 20X (**A, E**) and 40X (**B-D and F-H**). Scale bar: 500 µm.

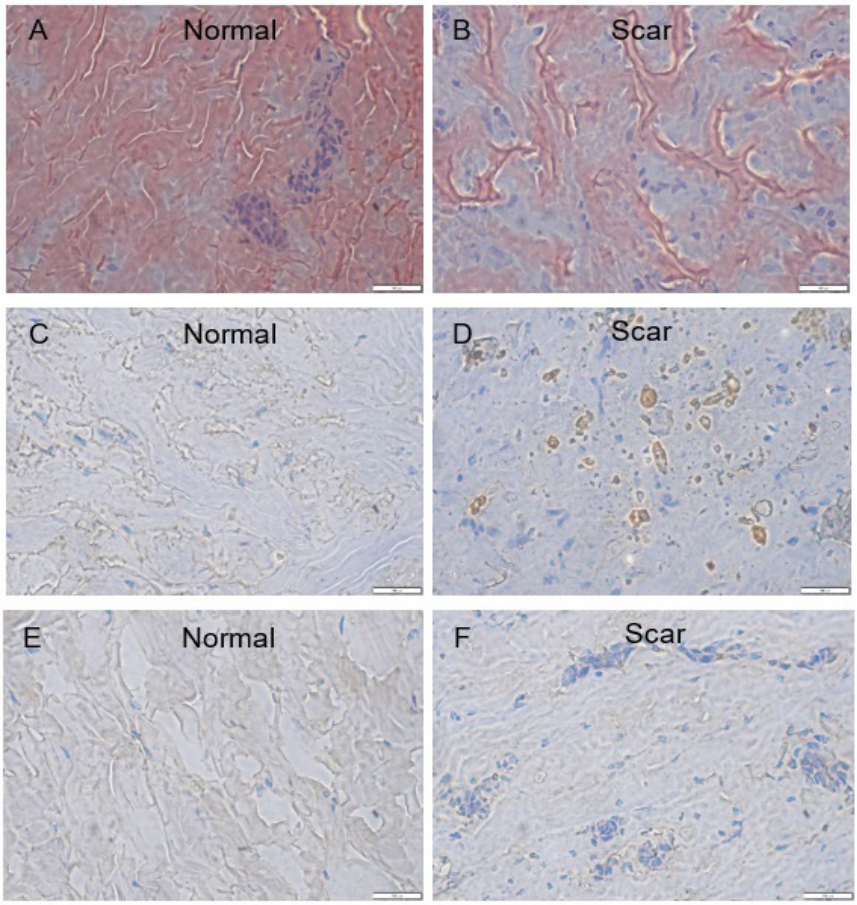

Figure 5: Disordered arrangement of collagen bundles, defects in autophagy function and inflammation in scar**.** Histopathological evaluation of tissues with Congo red staining. (**A**) Normal skin tissue (control) showed no abnormality, whereas (**B**) scar tissue showed aggregates of blood vessels and stretched collagen bundles. Evaluation of tissues with Beclin-1 autophagy marker. (**C**) Normal skin tissue showed (control) no abnormality, whereas (**D**) scar tissue showed cellular debris. Evaluation of tissues with IBA-1 inflammation marker. (**E**) Normal skin tissue (control) showed no abnormality, whereas (**F**) scar tissue showed aggregates of inflammatory cells. Magnification: 40X (**A-F**). Scale bar: 500 µm.

5. Concluding Remarks

We examined a case of hypertropic scarring on abdominal skin of a 36-year-old female. Comparison of a hypertrophic scar to surrounding normal tissue as revealed by DESI-MSI upregulation of phospholipid sphingomyelin SM(18:0/16:1), *m/z* 235.18, and upregulation of metabolite sphingosine, *m/z* 310.24 which suggest possible roles for these biomolecules in the development and maintenance of hypertrophic scars. Moreover, the scar tissue showed downregulation of phospholipid cardiolipin CL(62:2), *m/z* 1322.03 that suggested defects in autophagy function. Although this work represents only one case study, it does indicate the promise of DESI-MSI in combination with histopathological staining in understanding the molecular basis of the hypertrophic scarring process. We suggest that multiple skin samples in follow-up studies will be needed to draw definite conclusions, but we find that DESI-MSI might offer an excellent approach for understanding better the molecular basis of hypertrophic scarring.

References

1. Bordoni, B. and E. Zanier. Skin, fascias, and scars: symptoms and systemic connections. J Multidiscip Healthc. 2013 Dec 28; 7: 11-24.
2. Steiling H and Werner S. Fibroblast growth factors: key players in epithelial morphogenesis, repair and cytoprotection. Curr Opin Biotechnol. 2003; 14(5): 533-7.
3. Werner S and R Grose. Regulation of wound healing by growth factors and cytokines. Physiol Rev. 2003; 83(3): p. 835-70.
4. Huang BS, Horng HC, Yeh CC, Chen YJ. Wound healing. J Chin Med Assoc. 2018; 81(2): p. 94-101.
5. Yuan FL, Sun ZL, Feng Y, Liu SY, Du Y, Yu S, et al., Epithelial-mesenchymal transition in the formation of hypertrophic scars and keloids. J Cell Physiol. 2019. 234(12): p. 21662-21669.
6. Finnerty CC, Jeschke MG, Branski LK, Barret JP, Dziewulski P, Herndon DN, et al., Hypertrophic scarring: the greatest unmet challenge after burn injury. Lancet. 2016; 388(10052): p. 1427-1436.
7. Van Loey NE and Van Son MJ. Psychopathology and psychological problems in patients with burn scars: epidemiology and management. Am J Clin Dermatol. 2003; 4(4): p. 245-72.
8. Feng Y, Sun ZL, Liu SY, Wu JJ, Zhao BH, Lv GZ, et al. Direct and Indirect Roles of Macrophages in Hypertrophic Scar Formation. Front Physiol, 2019; 10: p. 1101.
9. Wilgus TA. Vascular Endothelial Growth Factor and Cutaneous Scarring. Adv Wound Care (New Rochelle), 2019; 8(12): p. 671-678.
10. Tu TH, Joe Y, Choi HS, Chung HT, Yu R. Induction of heme oxygenase-1 with hemin reduces obesity-induced adipose tissue inflammation via adipose macrophage phenotype switching. Mediators Inflamm, 2014; 2014: p. 290708.
11. Balazs L, J Okolicany, M Ferrebee, B Tolley, G Tigyi. Topical application of the phospholipid growth factor lysophosphatidic acid promotes wound healing in vivo. Am J Physiol Regul Integr Comp Physiol. 2001; 280(2): p. R466-72.
12. Wei S, LT Chow, IO Shum, L Qin, JE Sanderson. Left and right ventricular collagen type I/III ratios and remodeling post-myocardial infarction. J Card Fail. 1999; 5(2): p. 117-26.
13. Plikus MV, Guerrero-Juarez CF, Ito M, Li YR, Dedhia PH, Zheng Y Regeneration of fat cells from myofibroblasts during wound healing. Science. 2017; 355(6326): p. 748-752.
14. Mokos ZB, Jovic A, Grgurevic L, Dumic-Cule I, Kostovic K, Ceovic R, et al. Current Therapeutic Approach to Hypertrophic Scars. Front Med (Lausanne). 2017; 4: p. 83.
15. Ogawa R. Keloid and Hypertrophic Scars Are the Result of Chronic Inflammation in the Reticular Dermis. Int J Mol Sci. 2017; 18(3): 606.
16. Brown BC, S P McKenna, K Siddhi, D A McGrouther, A Bayat. The hidden cost of skin scars: quality of life after skin scarring. J Plast Reconstr Aesthet Surg. 2008; 61(9): p. 1049-58.
17. Li J, Wang J, Wang Z, Xia Y, Zhou M, Zhong A, et al. Experimental models for cutaneous hypertrophic scar research. Wound Repair Regen. 2020; 28(1): p. 126-144.
18. Domergue S, Jorgensen C and Noël D. Advances in Research in Animal Models of Burn-Related Hypertrophic Scarring. J Burn Care Res. 2015; 36(5): p. e259-66.
19. Ramos ML, Gragnani A and Ferreira LM. Is there an ideal animal model to study hypertrophic scarring? J Burn Care Res. 2008; 29(2): p. 363-8.
20. Hankin JA. Farias SE, Barkley RM, Heidenreich K, Frey LC, Hamazaki K, et al. MALDI mass spectrometric imaging of lipids in rat brain injury models. J Am Soc Mass Spectrom. 2011; 22(6): p. 1014-21.
21. Pulfer M and Murphy RC. Electrospray mass spectrometry of phospholipids. Mass Spectrom Rev. 2003; 22(5): p. 332-64.
22. Banerjee S, Zare RN, Tibshirani RJ, Kunder CA, Nolley R, Fan R, et al., Diagnosis of prostate cancer by desorption electrospray ionization mass spectrometric imaging of small metabolites and lipids. Proc Natl Acad Sci USA. 2017; 114(13): p. 3334-3339.
23. Ferreira CR, Dill AL, Ifa DR, Cheng L, Cooks RG. Nondestructive, histologically compatible tissue imaging by desorption electrospray ionization mass spectrometry. Chembiochem. 2011; 12(14): p. 2129-32.
24. Källback P, Nilsson A, Shariatgorji M, Andrén PE. msIQuant--Quantitation Software for Mass Spectrometry Imaging Enabling Fast Access, Visualization, and Analysis of Large Data Sets. Anal Chem. 2016; 88(8): p. 4346-53.
25. Tredget EE, Nedelec B, Scott PG, Ghahary A. Hypertrophic scars, keloids, and contractures. The cellular and molecular basis for therapy. Surg Clin North Am. 1997; 77(3): p. 701-30.
26. Folch J, Lees M and Sloane Stanley GH. A simple method for the isolation and purification of total lipides from animal tissues. J Biol Chem. 1957. 226(1): p. 497-509.

27. Zhu Z, Ding J and Tredget EE. The molecular basis of hypertrophic scars. Burns Trauma. 2016; 4: p. 2.
28. Carney BC, Chen JH, Kent RA, Rummani M, Alkhalil A, Moffatt LT, et al. Reactive Oxygen Species Scavenging Potential Contributes to Hypertrophic Scar Formation. J Surg Res. 2019; 244: p. 312-323.
29. Ţuţuianu R, Roşca AM, Florea G, Prună V, Iacomi DM, Rădulescu LA, et al. Heterogeneity of human fibroblasts isolated from hypertrophic scar. Rom J Morphol Embryol. 2019; 60(3): p. 793-802.
30. Gold MH, McGuire M, Mustoe TA, Pusic A, Sachdev M, Waibel J, et al. Updated international clinical recommendations on scar management: part 2--algorithms for scar prevention and treatment. Dermatol Surg. 2014; 40(8): p. 825-31.
31. Terashi H, K Izumi, L M Rhodes, C L Marcelo. Human stratified squamous epithelia differ in cellular fatty acid composition. J Dermatol Sci. 2000; 24(1): p. 14-24.
32. Graber R, C Sumida and EA Nunez, Fatty acids and cell signal transduction. J Lipid Mediat Cell Signal. 1994; 9(2): p. 91-116.
33. Lei L, Su J, Chen J, Chen W, Chen X, Peng C. The role of lysophosphatidic acid in the physiology and pathology of the skin. Life Sci. 2019; 220: p. 194-200.
34. van Blitterswijk WJ, van der Meer BW and Hilkmann H. Quantitative contributions of cholesterol and the individual classes of phospholipids and their degree of fatty acyl (un)saturation to membrane fluidity measured by fluorescence polarization. Biochemistry. 1987; 26(6): p. 1746-56.
35. Wattenberg BW and Silbert DF. Sterol partitioning among intracellular membranes. Testing a model for cellular sterol distribution. J Biol Chem. 1983; 258(4): p. 2284-9.
36. Baumer Y, Ng Q, Sanda GE, Dey AK, Teague HL, Sorokin AV, et al. Chronic skin inflammation accelerates macrophage cholesterol crystal formation and atherosclerosis. JCI Insight. 2018; 3(1): e97179.
37. Antón Z, Landajuela A, Hervás JH, Montes LR, Hernández-Tiedra S, Velasco G, et al., Human Atg8-cardiolipin interactions in mitophagy: Specific properties of LC3B, GABARAPL2 and GABARAP. Autophagy. 2016; 12(12): p. 2386-2403.
38. Nixon RA. The role of autophagy in neurodegenerative disease. Nat Med. 2013; 19(8): p. 983-97.
39. Kubli DA and Gustafsson AB, Mitochondria and mitophagy: the yin and yang of cell death control. Circ Res. 2012; 111(9): p. 1208-21.
40. Lu H, Guangliang Li, Leiming Liu, Lifeng Feng, Xian Wang, Hongchuan Jin. Regulation and function of mitophagy in development and cancer. Autophagy. 2013; 9(11): p. 1720-36.
41. Gauglitz GG, Korting HC, Pavicic T, Ruzicka T, Jeschke MG. Hypertrophic scarring and keloids: pathomechanisms and current and emerging treatment strategies. Mol Med. 2011; 17(1-2): p. 113-25.
42. Moshref S and Mufti S. Keloid and Hypertrophic Scars: Comparative Histopathological and Immunohistochemical Study. Med Sci. 2009; 17.
43. Verhaegen PD, Zuijlen PPMV, Pennings NM, Marle JV, Niessen FB, Horst CMAMVD, et al. Differences in collagen architecture between keloid, hypertrophic scar, normotrophic scar, and normal skin: An objective histopathological analysis. Wound Repair Regen. 2009; 17(5): p. 649-56.
44. Tuan TL and Nichter LS. The molecular basis of keloid and hypertrophic scar formation. Mol Med Today. 1998; 4(1): 19-24.
45. Chu CT, Ji J, Dagda RK, Jiang JF, Tyurina YY, Kapralov AA, et al. Cardiolipin externalization to the outer mitochondrial membrane acts as an elimination signal for mitophagy in neuronal cells. Nat Cell Biol. 2013; 15(10): p. 1197-1205.